atmosphere

MDPI

Article

The Different Impacts of Emissions and Meteorology on $PM_{2.5}$ Changes in Various Regions in China: A Case Study

Wenjie Zhang [1,2], Hong Wang [2,*], Xiaoye Zhang [2], Yue Peng [2], Zhaodong Liu [2], Junting Zhong [2], Yaqiang Wang [2], Huizheng Che [2] and Yifan Zhao [2]

[1] Department of Atmospheric and Oceanic Sciences and Institute of Atmospheric Sciences, Fudan University, Shanghai 200433, China; 20113020027@fudan.edu.cn

[2] State Key Laboratory of Severe Weather and Key Laboratory of Atmospheric Chemistry of CMA, Chinese Academy of Meteorological Sciences, Beijing 100081, China; xiaoye@cma.gov.cn (X.Z.); 20181102036@nuist.edu.cn (Y.P.); 20201103009@nuist.edu.cn (Z.L.); zhongjt@cma.gov.cn (J.Z.); yqwang@cma.gov.cn (Y.W.); chehz@cma.gov.cn (H.C.); zhaoyifan20@mails.ucas.ac.cn (Y.Z.)

* Correspondence: wangh@cma.gov.cn

Abstract: Emissions and meteorology are significant factors affecting aerosol pollution, but it is not sufficient to understand their relative contributions to aerosol pollution changes. In this study, the observational data and the chemical model (GRAPES_CUACE) are combined to estimate the drivers of $PM_{2.5}$ changes in various regions (the Beijing–Tianjin–Hebei (BTH), the Central China (CC), the Yangtze River Delta (YRD), and the Pearl River Delta (PRD)) between the first month after COVID-19 (FMC_2020) (i.e., from 23 January to 23 February 2020) and the corresponding period in 2019 (FMC_2019). The results show that $PM_{2.5}$ mass concentration increased by 26% (from 61 to 77 $\mu g\ m^{-3}$) in the BTH, while it decreased by 26% (from 94 to 70 $\mu g\ m^{-3}$) in the CC, 29% (from 52 to 37 $\mu g\ m^{-3}$) in the YRD, and 32% (from 34 to 23 $\mu g\ m^{-3}$) in the PRD in FMC_2020 comparing with FMC_2019, respectively. In the BTH, although emissions reductions partly improved $PM_{2.5}$ pollution (−5%, i.e., $PM_{2.5}$ mass concentration decreased by 5% due to emissions) in FMC_2020 compared with that of FMC_2019, the total increase in $PM_{2.5}$ mass concentration was dominated by more unfavorable meteorological conditions (+31%, i.e., $PM_{2.5}$ mass concentration increased by 31% due to meteorology). In the CC and the YRD, emissions reductions (−33 and −36%) played a dominating role in the total decrease in $PM_{2.5}$ in FMC_2020, while the changed meteorological conditions partly worsened $PM_{2.5}$ pollution (+7 and +7%). In the PRD, emissions reductions (−23%) and more favorable meteorological conditions (−9%) led to a total decrease in $PM_{2.5}$ mass concentration. This study reminds us that the uncertainties of relative contributions of meteorological conditions and emissions on $PM_{2.5}$ changes in various regions are large, which is conducive to policymaking scientifically in China.

Keywords: $PM_{2.5}$; meteorological conditions; emissions reductions; different regions in China

check for updates

Citation: Zhang, W.; Wang, H.; Zhang, X.; Peng, Y.; Liu, Z.; Zhong, J.; Wang, Y.; Che, H.; Zhao, Y. The Different Impacts of Emissions and Meteorology on $PM_{2.5}$ Changes in Various Regions in China: A Case Study. *Atmosphere* **2022**, *13*, 222. https://doi.org/10.3390/atmos13020222

Academic Editor: Begoña Artíñano

Received: 27 December 2021
Accepted: 26 January 2022
Published: 28 January 2022

1. Introduction

$PM_{2.5}$ pollution has serious impacts on human daily life and health by affecting radiation, visibility, the ecological environment, etc. [1–5], which has attracted widespread attention in China.

$PM_{2.5}$ pollution in China is closely related to anthropogenic emissions [6–9]. Combustion sources (coal combustion, traffic emissions, industrial emissions, biomass burning, etc.) have made significant contributions to aerosol pollution over the past several years [10–13]. In the past, coal combustion contributed to more than 50% of $PM_{2.5}$ emissions during the winter in Northern China [14,15]. However, traffic emissions have increasingly become the largest source of $PM_{2.5}$ emissions and account for 40 to 60% [11,12,16]. Secondary aerosol formation also can contribute significantly to elevated $PM_{2.5}$ mass concentration, accounting for 50 to 70% of the aerosol components during the heavy aerosol pollution episodes (HPEs) [17–20].

In addition to emissions, meteorological conditions also have important impacts on $PM_{2.5}$ concentration by changing the ventilation rate, dry/wet deposition, chemical conversion loss rate, etc. [21–23]. Zonal westerly airflow and high-pressure ridge are two major background circulations that cause a reduction in the height of the planetary boundary layer (PBLH), affecting the formation of aerosol pollution in the Beijing–Tianjin–Hebei (BTH) [24]. Under normal circumstances, the appearance of weaker wind speed (WS), higher relative humidity (RH), and temperature inversion can be conducive to the accumulation of aerosol pollution in Beijing, Nanjing, Guangzhou, Sichuan Basin, etc. [25–28]. Some studies show that increasing wind speed will enhance $PM_{2.5}$ mass concentration by a transmission and convergence process [29,30]. It should also be noted that when the $PM_{2.5}$ accumulates to a certain level, it will further worsen the meteorological conditions [31,32]. A significant "two-way feedback" effect between $PM_{2.5}$ and unfavorable meteorological conditions for aerosol pollution diffusion is determined by studying the formation of HPEs in multiple cities in China [33–35].

Emissions and meteorological conditions will both affect the changes in $PM_{2.5}$ mass concentration, but the question of which parameter is more important is still the focus of research [21,36–39]. In the past few years, the Chinese government has implemented a series of air pollution control measures, such as the "Action Plan on Prevention and Control of Air Pollution", the "Three-year Action Plan for Blue Skies", etc. [40–43]. Under the influence of control measures, the $PM_{2.5}$ pollution has been greatly improved. Most studies show that emissions reductions play a dominant role (about 70–80%) in the improvement of air quality from 2013 to 2017 [21,38,39]. However, some studies also pointed out that the contributions of changed meteorological conditions to the improvement of $PM_{2.5}$ reach about 50% in winter [44,45]. Moreover, even in the background of continuous emissions reductions, HPEs still occur in many cities in China due to unfavorable meteorological conditions for aerosol pollution diffusion and secondary formation [46–48]. All of these fully illustrate the complicated non-linear relationship between $PM_{2.5}$ concentration, meteorological conditions, and pollutants emissions. During the COVID-19 outbreak period, various anthropogenic emissions showed a significant decrease [49–52], e.g., large reductions in NO_2 were caused by the significantly reduced traffic emissions [52,53]. This special lockdown situation provided a better opportunity to study the relationship between $PM_{2.5}$ and emissions and meteorological conditions in China.

Although many studies have carried out some work about the reasons for changes in emissions, major air pollutants concentration, and aerosol composition during the COVID-19 outbreak in China [53–57], they are only for a certain element or region. The comprehensive study of the causes of $PM_{2.5}$ changes during the COVID-19 outbreak is still poor, especially the comparisons in various regions. In this study, air pollutants data, meteorological data, and the GRAPES_CUACE model are used to investigate reasons for $PM_{2.5}$ mass concentration changes during the first month (from 23 January to 23 February 2020) after COVID-19 (FMC_2020) compared with the corresponding historical period in 2019 (FMC_2019) in China. The discussions help further understand the causes of aerosol pollution changes in various regions and provide scientific technique support for regional aerosol pollution control in China.

2. Materials and Methods

2.1. Air Pollutants Data

Hourly major air pollutants ($PM_{2.5}$, CO, NO_2, and SO_2) mass concentration in FMC_2019 and FMC_2020 are collected by an automated ambient air quality monitoring system (an air quality monitoring sub-station, a quality assurance laboratory, etc.) from the Ministry of Ecology and Environment of China. This system can automatically monitor, collect, process, and store $PM_{2.5}$ and gaseous pollutants data, then transmit data to the central computer, and finally collate data by quality assurance process (invalid data should have raw records).

The mass concentration units are μg m^{-3} for $PM_{2.5}$, NO_2, SO_2, and mg m^{-3} for CO. For the missing data, if the sample size is sufficient, we choose to directly remove the missing data. If the sample size is insufficient, we use adjacent data to supplement [58].

2.2. Meteorological Data

Meteorological data come from National Centers for Environmental Prediction (NCEP) Final (FNL) analysis data. This product is conducted by the Global Data Assimilation System (GDAS), which continuously collects observational data from the Global Telecommunications System (GTS), and other sources. The FNL analysis data are made with the same model which NCEP uses in the Global Forecast System (GFS), but the FNL analysis data are delayed so that more observational data (e.g., satellite data and radar data) can be used. We use the FNL analysis data in FMC_2019 and FMC_2020 with the resolution of 0.25° × 0.25° in this paper. These data mainly include geopotential height, sea level pressure, PBLH, temperature (T), RH, and WS.

2.3. Study Regions

This study focuses on the comparative analysis of the four major megacity clusters (the BTH, the Yangtze River Delta (YRD), the Pearl River Delta (PRD), and the Central China (CC)) (Figure 1). The aerosol pollution in the BTH (38° N–42° N, 113° E–120° E), the YRD (29° N–33° N, 118° E–122° E), the PRD (21° N–25° N, 110° E–115° E), and the CC (28° N–35° N, 109° E–116° E) has been extensively studied, which are the four typical pollution regions in China.

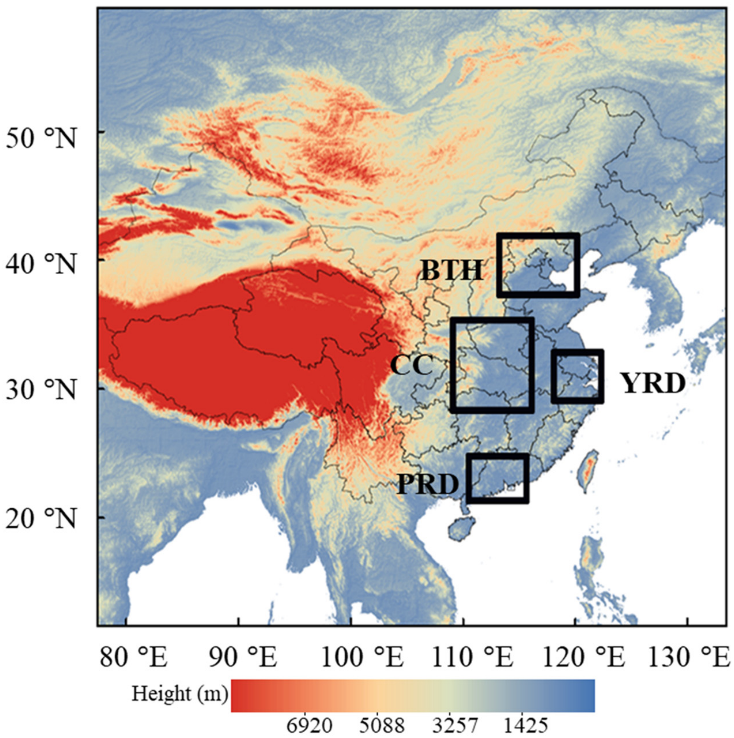

Figure 1. The four study regions in China including the BTH, the CC, the YRD, and the PRD. The shadow represents the height of the terrain (m).

2.4. Statistical Analysis

In a certain period, primary $PM_{2.5}$ and gas pollutants generally have the same anthropogenic emissions, and the contribution ratio of emissions to them is relatively stable, so gas pollutants can be used to estimate impacts of emissions changes on $PM_{2.5}$ [59–61]. For the primary source of $PM_{2.5}$, the influence of combustion sources is mainly studied. Among the main gas pollutants, CO is selected as an indicator of the primary combustion sources [62,63], because CO has a long lifetime and is less affected by chemical reactions [63–66]. In addition, we use a linear relationship to fit CO and $PM_{2.5}$ mass concentration with a determination coefficient (r^2). The r^2 reflects how much the changes of CO mass concentration can account for $PM_{2.5}$ changes, as shown in Equation (1):

$$r^2 = \frac{\sum(\dot{y}_i - \overline{y})^2}{\sum(y_i - \overline{y})^2} \quad (1)$$

where i is the ith sample, $\dot{y}_i$ and y_i represent the $PM_{2.5}$ mass concentration calculated by the linear fitting equation and the actual $PM_{2.5}$ mass concentration, respectively, and $\overline{y}$ is the mean $PM_{2.5}$ mass concentration.

Here we assume that the changes of air pollutants are only affected by emissions and meteorological conditions, which is a general method in many studies. Therefore, the changes in CO and $PM_{2.5}$ mass concentration under similar meteorological conditions are used to represent the contributions of emissions.

2.5. Model

GRAPES_CUACE is a chemical weather model which is online coupled by the mesoscale weather model (the Global–Regional Assimilation and Prediction System, i.e., GRAPES_Meso) and the chemical module (the Chinese Unified Atmospheric Chemistry Environment, i.e., CUACE) [67–69]. GRAPES_Meso model is an operational regional numerical weather prediction model independently developed by China Meteorological Administration (CMA) [70–72]. CUACE mainly includes four parts: emissions, gas-phase chemistry, aerosols, and data assimilation [67]. GRAPES_CUACE model has been widely used in studying the interactions between aerosol and meteorology, aerosol pollution transport, pollutants forecast, etc. [73–75].

The assimilation system of GRAPES_CUACE model is formed by the Three-Dimensional Variational Assimilation (3DVAR) and the Four-Dimensional Variational Assimilation (4DVAR), which is optional. In this study, we use 3DVAR to perform data assimilation [71]. The physical and chemical schemes selected in this model are the same as those in Zhang et al. [76]. These schemes are listed in Table 1. There are 7 species of aerosol that can be modeled, including sulfates, soil dust, black carbon, organic carbon, sea salts, nitrates, and ammonium salts. The initial and boundary conditions are provided by FNL reanalysis data ($0.25° \times 0.25°$), and the emissions used in the model are Multi-resolution Emission Inventory for China (MEIC) of Tsinghua University in 2017 [7,59]. The anthropogenic emissions used in the model are Multi-resolution Emission Inventory for China (MEIC) of Tsinghua University in 2017. MEIC covers more than 700 anthropogenic emissions in the whole of China, which has 10 major atmospheric pollutants and carbon dioxide (SO_2, NO_x, CO, NMVOC, NH_3, $PM_{2.5}$, PM_{10}, BC and OC, CO_2). The natural emissions do not enter into the current model. Usually, the contributions of anthropogenic emissions to aerosol pollution are much greater than those of natural emissions. In the future, we will consider natural emissions in the model to simulate air pollution accurately. The simulated area includes the entire Chinese region and the two simulated periods are FMC_2019 and FMC_2020. The model has a horizontal resolution of $0.15° \times 0.15°$ and a vertical resolution of 31 levels (from 1000 hPa to 1 hPa).

It is worth noting that we cannot evaluate the simulations in this study because the emissions and the simulated period are not in the same years. However, the model simulations by using the emissions and the meteorology in the same year have been widely validated in the paper of Zhang et al. [76], which indicates that the GRAPES_CUACE model can be used to simulate changes in meteorology and $PM_{2.5}$ and the results are credible. The descriptions of sensitive experiments are shown in Table 2 and the difference between the two experiments (EXP1 and EXP2) can determine the impact of meteorological conditions on $PM_{2.5}$ changes.

Table 1. Physical and chemical schemes.

Schemes Option	References
Noah land surface	(Chen and Dudhia) [77]
WSM6 cloud microphysics	(Hong and Lim) [78]
RRTM long-wave radiation	(Mlawer et al.) [79]
Goddard short-wave radiation	(Chou et al.) [80]
Monin-Obukhov near-ground layer	(Chen et al.) [81]
MRF boundary layer	(Hong and Pan) [82]
RADM2 gas-phase chemistry	(Stockwell et al.) [83]
CUACE aerosol process	(Zhou et al.) [84]

Table 2. The descriptions of sensitive experiments.

Experiment	Description
EXP1	Model runs with FMC_2019 meteorology and 2017 emission
EXP2	Model runs with FMC_2020 meteorology and 2017 emission

3. Results

3.1. Changes in $PM_{2.5}$ Mass Concentration from FMC_2019 to FMC_2020

Figure 2 shows the distributions of $PM_{2.5}$ mass concentration in China in FMC_2020 and FMC_2019. In FMC_2019, the highest monthly average $PM_{2.5}$ mass concentration is 94 μg m^{-3} in the CC, followed by 61 μg m^{-3} in the BTH, 52 μg m^{-3} in the YRD, and 34 μg m^{-3} in the PRD (Figure 2a). Compared with FMC_2019, the $PM_{2.5}$ mass concentration in the CC, the YRD, and the PRD regions decrease to 70, 37, 23 μg m^{-3} (26, 29, and 32% less than the $PM_{2.5}$ mass concentration in FMC_2019) in FMC_2020 (Figure 2b–d). However, $PM_{2.5}$ mass concentration in the BTH unexpectedly increases to 77 μg m^{-3} (26% more than the $PM_{2.5}$ mass concentration in FMC_2019) (Figure 2b–d). In general, the $PM_{2.5}$ pollution levels in the BTH and the CC are higher than those in the YRD and the PRD.

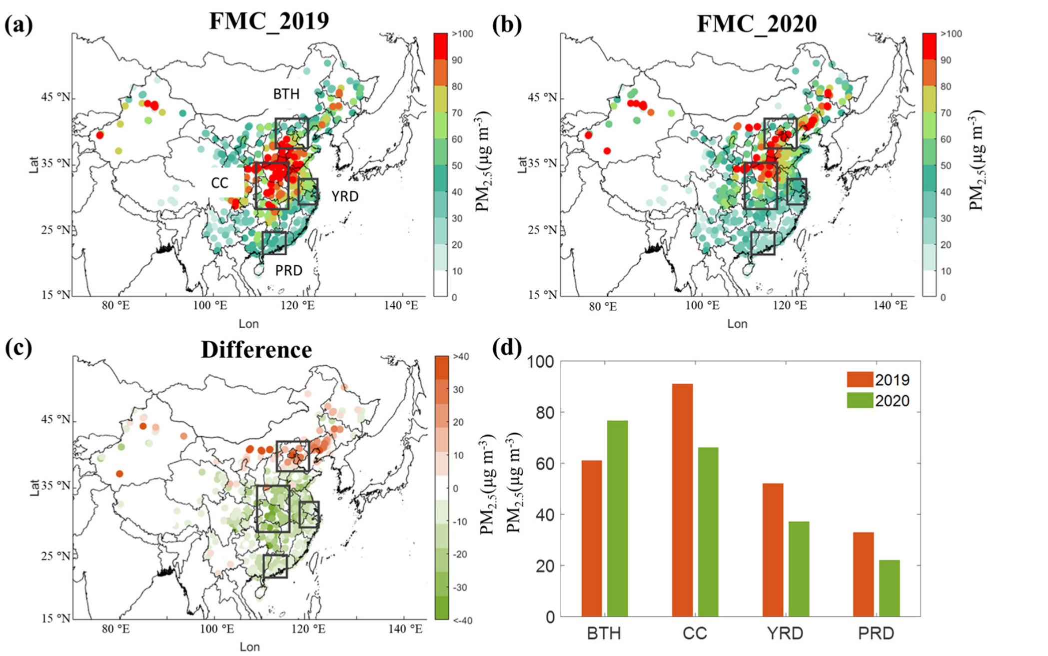

Figure 2. Distributions of monthly average $PM_{2.5}$ mass concentration (μg m^{-3}) in China. (**a**) FMC_2019. (**b**) FMC_2020. (**c**) Difference of $PM_{2.5}$ mass concentration between FMC_2019 and FMC_2020. (**d**) The histogram of $PM_{2.5}$ mass concentration in the BTH, the CC, the YRD, and the PRD.

3.2. Impacts of Anthropogenic Emissions on $PM_{2.5}$ Mass Concentration Changes from FMC_2019 to FMC_2020

Figure 3a,b is the spatial distribution of CO in China. Compared with FMC_2019, CO mass concentration has a small decrease in FMC_2020. The overall CO mass concentration in the CC, the YRD, and the PRD has decreased by 14, 12, and 21%, but the CO mass concentration in the BTH has increased by 10% (Table 3). The changes in CO mass concentration in these four regions are mainly affected by primary sources and meteorological conditions. To eliminate the influence of meteorological conditions and the possibility of transportation [85], we select periods for analysis that are associated with stable and similar meteorological conditions between FMC_2019 and FMC_2020 in four regions as much as possible (Table 4). For example, the meteorological conditions affecting BTH during 28–29 January and 1–2 February 2019 are similar to those during 9–11 February and 19–20 February 2020. The difference of mean atmospheric compositions between the periods in FMC_2019 and FMC_2020 can indicate the net effectiveness of large-scale lockdown measures after the COVID-19 outbreak. The same methods are also used in the CC, the YRD, and the PRD. The long-range transport of CO can be excluded in Figures S3–S6. The comparison results show that CO mass concentration from primary sources decreases by about 4, 18, 15, and 10% in the BTH, the CC, the YRD, and the PRD in FMC_2020 compared with FMC_2019 (Table 4), which means that the combustion sources reductions are relatively smaller in the BTH and larger in the CC than other regions.

Table 3. Regional monthly average gas pollutants (CO, NO_2, SO_2) mass concentration in FMC_2019 and FMC_2020.

Area	CO (mg m^{-3})		NO_2 (µg m^{-3})		SO_2 (µg m^{-3})	
	2019	2020	2019	2020	2019	2020
BTH	1.16	1.26	37.90	29.01	20.04	16.21
CC	1.13	0.97	31.58	16.62	11.43	7.91
YRD	0.82	0.72	34.53	18.24	8.08	6.33
PRD	0.86	0.68	26.37	15.21	7.11	5.78

Table 4. The average CO mass and $PM_{2.5}$ mass concentration during periods associated with similar stable meteorological conditions in FMC_2019 and FMC_2020.

Periods	Major Influencing Weather Systems	Average CO Mass Concentration (mg m^{-3})	Average $PM_{2.5}$ Mass Concentration (µg m^{-3})
BTH			
28–29 January 2019 1–2 February 2019	BTH is controlled by a strong high ridge at 500 hPa and uniform sea level pressure. Then the high ridge moves eastward.	1.61	95
9–11 February 2020 19–20 February 2020		1.55	89
CC			
27–28 January 2019 17–20 February 2019	CC is controlled by zonal westerly airflow at 500 hPa and relatively weaker sea level pressure gradient.	1.2	109
1–4 February 2020		0.98	82
YRD			
27–28 January 2019 16–17 February 2019	YRD is basically controlled by zonal westerly airflow at 500 hPa and relatively weaker sea level pressure gradient.	0.83	53
1–4 February 2020		0.71	36
PRD			
28 January 2019– 1 February 2019	PRD is controlled by a weak high ridge with continuous movement to eastward at 500 hPa. The relatively weaker sea level pressure gradient influences PRD.	0.84	49
10–12 February 2020		0.76	39

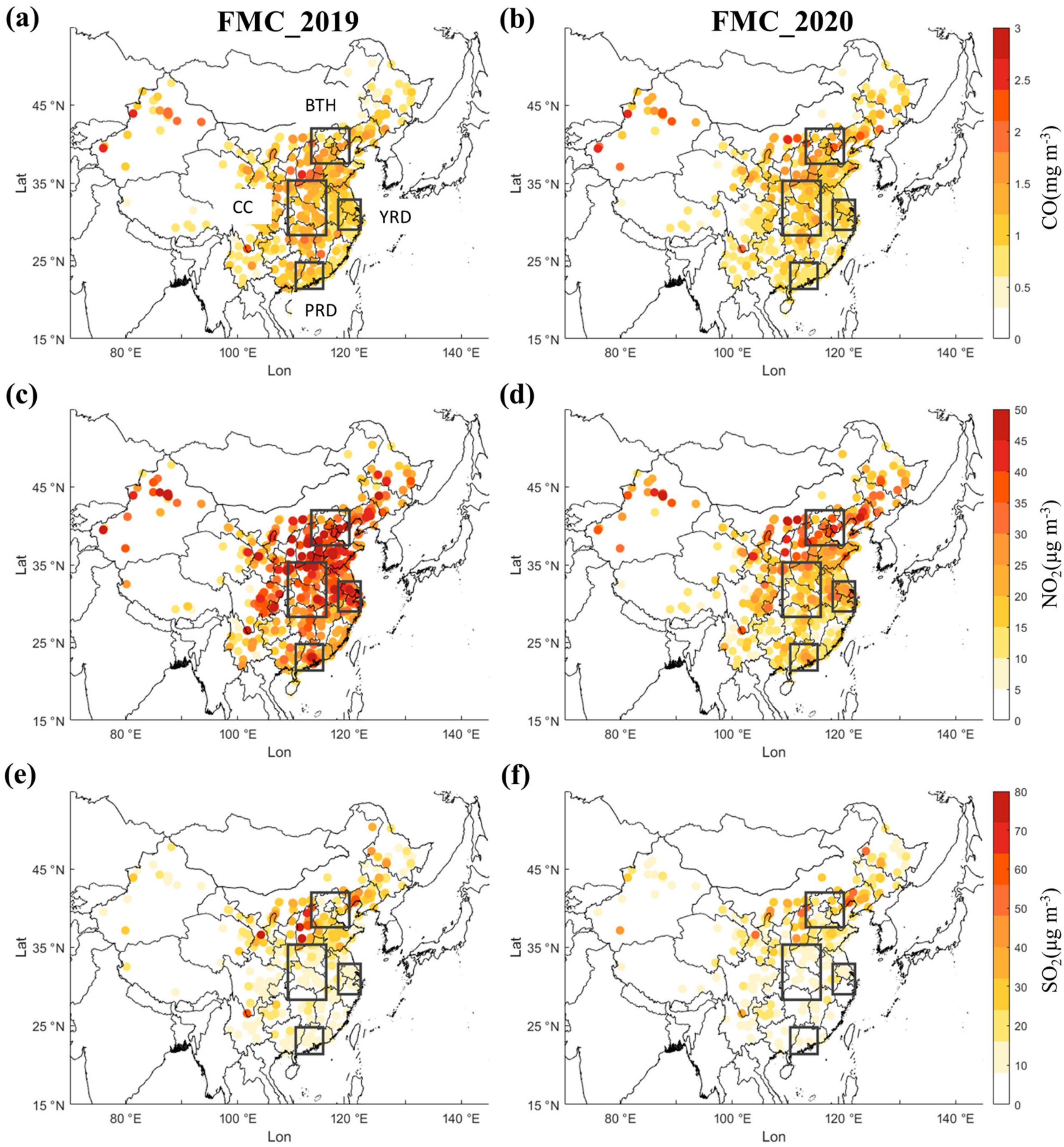

Figure 3. Distributions of monthly average gas pollutants mass concentration (μg m^{-3} for NO_2 and SO_2, and mg m^{-3} for CO) in FMC_2019 and FMC_2020 in China. (**a**,**b**) CO. (**c**,**d**) NO_2. (**e**,**f**) SO_2.

In addition, Figure 4 shows the linear correlation between CO and $PM_{2.5}$. CO and $PM_{2.5}$ in the BTH, the CC, and the YRD have a strong positive correlation ($r^2 > 0.6$), while the correlation in the PRD is weak ($r^2 < 0.3$). All of these passed the 0.05 significance test. These show that $PM_{2.5}$ and CO in the BTH, the CC, and the YRD have similar sources, which means combustion sources have large contributions to $PM_{2.5}$. $PM_{2.5}$ in the PRD may be mainly affected by non-combustion sources, secondary aerosol, etc. Through calculations by the linear regression equations with different r^2 (Figure 4), compared with FMC_2019, the primary $PM_{2.5}$ from combustion sources increases by about 15% in the BTH, 18% in the CC, and decreases by 38% in the YRD, 83% in the PRD, which is consistent with previous studies about primary $PM_{2.5}$ [51,56]. Furthermore, the correlations analysis also finds that the increase in primary $PM_{2.5}$ from combustion sources in the BTH is closely related to the increase in the contribution of coal combustion (r^2 between SO_2 and $PM_{2.5}$ increases from 0.22 in FMC_2019 to 0.46 in FMC_2020). In the CC, the increase in the primary $PM_{2.5}$ from combustion sources is mainly related to NOx emissions (r^2 between NO_2 and $PM_{2.5}$ increases from 0.14 in FMC_2019 to 0.42 in FMC_2020), but it has been confirmed that the total primary emissions of $PM_{2.5}$ decrease (Table 4), indicating a more significant decrease in $PM_{2.5}$ from non-combustion sources. The lower contributions from combustion sources in the YRD and the PRD are mainly related to the decreased contributions of SO_2 related emissions (r^2 between SO_2 and $PM_{2.5}$ decreases from 0.44 (0.64) in FMC_2019 to 0.17 (0.18) in FMC_2020 in YRD (PRD)).

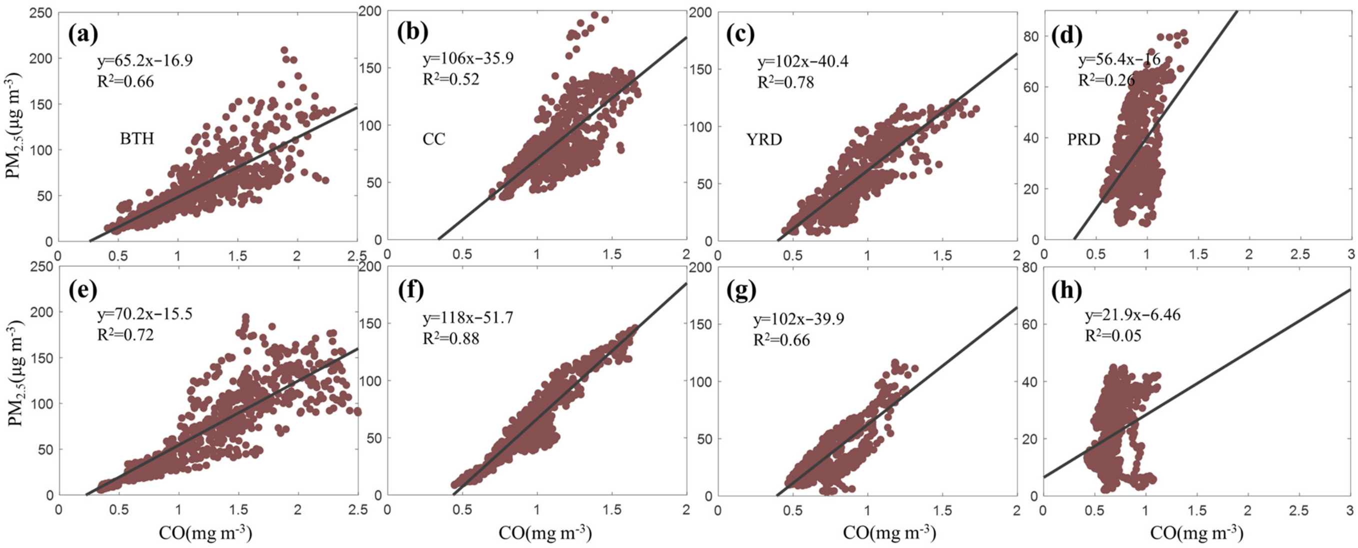

Figure 4. The linear correlations between CO and $PM_{2.5}$ mass concentration (µg m^{-3} for $PM_{2.5}$ and mg m^{-3} for CO) in the BTH, the CC, the YRD and the PRD. (**a**–**d**) FMC_2019. (**e**–**h**) FMC_2020.

In China, nitrate and sulfate are the most important components of secondary particulate matter in $PM_{2.5}$, which is partly affected by NOx and SO_2 in the air [86,87]. Figure 3c–f shows the spatial distribution of NO_2 mass concentration and SO_2 mass concentration in China in FMC_2019 and FMC_2020. It can be seen that compared with FMC_2019, NO_2 mass concentration and SO_2 mass concentration in China in FMC_2020 decrease significantly. The overall average NO_2 mass concentration in the BTH, the CC, the YRD, and the PRD regions decrease by 23, 47, 47, and 42%, and the SO_2 mass concentration decrease by 19, 31, 22, and 19%, respectively (Table 3). Correspondingly, the primary emissions of NOx and SO_2 in the four regions in FMC_2020 also show a downward trend, which is also confirmed by other studies [54]. The ratio of SO_2/NO_2 is one indicator of air pollution sources from mobile sources and stationary sources [88,89]. Figure 5 is the values of SO_2/NO_2. The highest value of SO_2/NO_2 is in the BTH, followed by the CC, the PRD, and the YRD, which shows that industrial emissions and coal combustion have a more significant impact on air pollution in the BTH in winter. At the same time, compared with two years, the value of SO_2/NO_2 in the BTH has changed a little, indicating that the impacts of mobile sources and stationary sources on air pollution are similar between FMC_2019 and FMC_2020. In the other three regions, the values of SO_2/NO_2 all increase in FMC_2020, indicating that air pollution is mainly influenced by stationary sources. The value of $PM_{2.5}/CO$ is also often used to measure the impacts of aerosol secondary formation processes on $PM_{2.5}$ [58,66]. Therefore, values of $PM_{2.5}/CO$ are calculated in the BTH, the CC, the YRD, and the PRD in FMC_2019 (0.049, 0.074, 0.053, and 0.037) and FMC_2020 (0.054, 0.062, 0.046, and 0.031). The degree of correlation between CO and $PM_{2.5}$ is not very high ($r^2 < 0.3$) in the PRD, so aerosol secondary formations are not well determined by the ratio and are, therefore, not very meaningful. The secondary aerosol formations in the BTH and the CC show higher contributions to $PM_{2.5}$ than those in the PRD and the YRD. Compared with FMC_2019, the weakening secondary aerosol formation processes in the air in FMC_2020 are mainly related to the substantial decrease in NOx and SO_2. It is worth noting that although primary emissions of NOx and SO_2 in the BTH have also been reduced, the secondary contributions to $PM_{2.5}$ are strengthened, which is consistent with previous studies [19,90]. For example, although the NOx emissions have decreased, the secondary aerosol formation process is still strengthened under unfavorable meteorological conditions for aerosol pollution diffusion, mainly due to the increased particle acidity (pH), which offsets the emissions reductions [19,90].

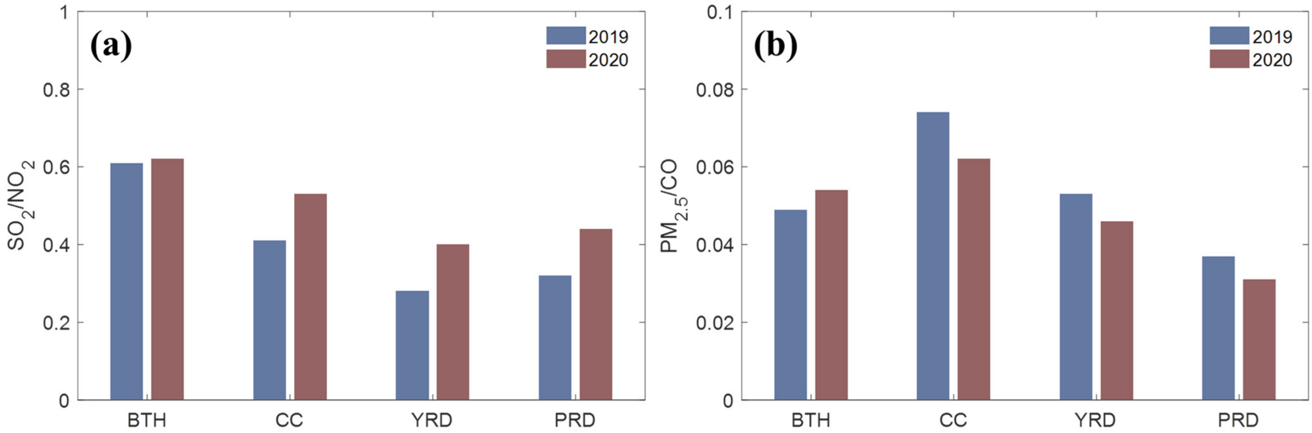

Figure 5. The values of SO_2/NO_2 (**a**) and $PM_{2.5}/CO$ (**b**) in the BTH, the CC, the YRD, and the PRD.

From the perspective of the contributions of all emissions changes to $PM_{2.5}$, we calculate the $PM_{2.5}$ mass concentration under similar meteorological conditions (Table 4). Compared with FMC_2019, $PM_{2.5}$ mass concentration decreases by 6, 25, 32, and 21% in the BTH, the CC, the YRD, and the PRD in FMC_2020. To a certain extent, there are still many uncertainties in the calculations. On the one hand, the impacts of meteorological conditions cannot be completely eliminated. On the other hand, the secondary formation processes of aerosol are greatly affected by meteorological conditions. For example, there are more secondary aerosols generated under unfavorable meteorological conditions for aerosol pollution diffusion [90]. All of these will lead to errors. However, there is a certain reference value when comparing the contributions of the two-year emissions changes to $PM_{2.5}$. Further research is needed.

3.3. Effects of Changes in Meteorological Conditions on $PM_{2.5}$ Mass Concentration from FMC_2019 to FMC_2020

Meteorological conditions also have a significant impact on affecting $PM_{2.5}$ pollution [21,46]. Figure 6 shows the background circulation patterns in FMC_2019 and FMC_2020. In FMC_2019, there is a strong Siberian–Mongolian high pressure with a central value of more than 1040 hPa. Eastern China is affected by this high-pressure system, causing clean and cold air from the north. At the same time, the 500 hPa geopotential height lines are relatively dense and the development of a high-pressure ridge is weak, which leads to poor atmospheric stability. In this case, it is beneficial to the horizontal and vertical diffusion of air pollutants. In FMC_2020, the Siberian–Mongolian high pressure becomes weaker and the central value is about 1035 hPa. The sea-level pressure in the four regions in China decreases significantly and becomes uniform. However, in the PRD, the gradient of sea-level pressure becomes larger, which is beneficial to the diffusion of air pollutants. At 500 hPa, the geopotential height lines are less dense than those in FMC_2019, and the development of the high-pressure ridge is strengthened, which leads to relatively strong atmospheric stability. These unfavorable meteorological conditions are conducive to the accumulation of aerosol pollution.

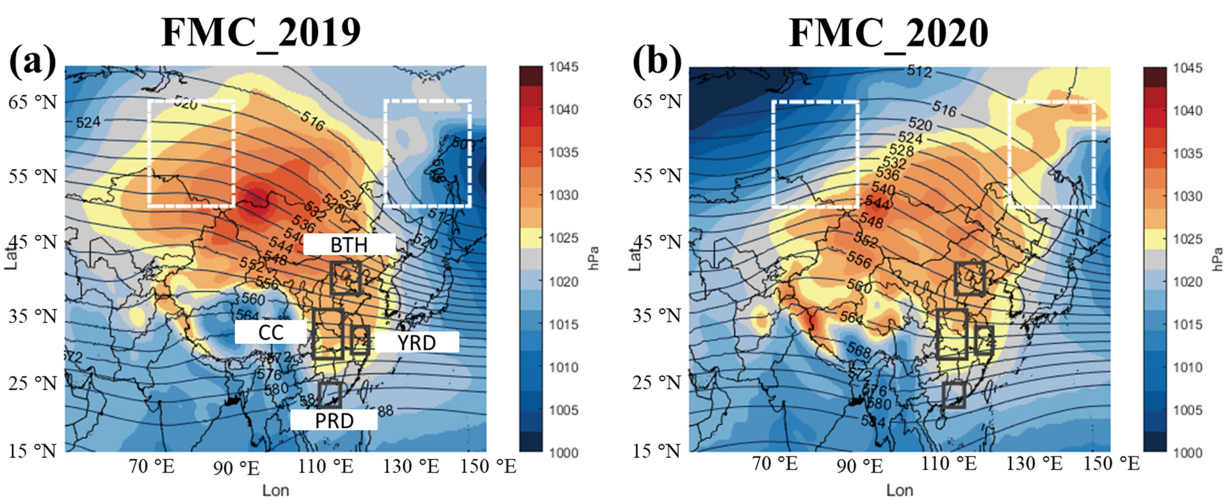

Figure 6. Monthly average geopotential height at 500 hPa and sea-level pressure over Eurasia. (**a**) FMC_2019; (**b**) FMC_2020. The white boxes are meridional circulation regions.

The meridional circulation index (MCI) is used to represent the intensity of atmospheric circulation [91,92]. The higher value of MCI means that it is easier for cold air from the north to flow to the south, and the exchange of airflow between north and south is enhanced, which is conducive to the diffusion of aerosol pollution. In this paper, we choose two regions for calculating MCI (50–65° N, 70–90° E and 50–65° N, 126–146° E, white boxes in Figure 6), which is consistent with the previous research [93]. Figure 7 shows the values of MCI at 400 and 500 hPa in FMC_2019 and FMC_2020. It can be seen that compared with FMC_2019, the MCI at 400 and 500 hPa in FMC_2020 has decreased by 38% (from 21 to 13) and 29% (from 24 to 17), respectively. This shows that the meridional circulation is significantly weaker in FMC_2020 and impacts of clean and cold air from the north on $PM_{2.5}$ are weakened, which is not conducive to the removal of aerosol pollution. The influence of the meridional circulation on the four regions of China is weakened one by one from the BTH to the PRD.

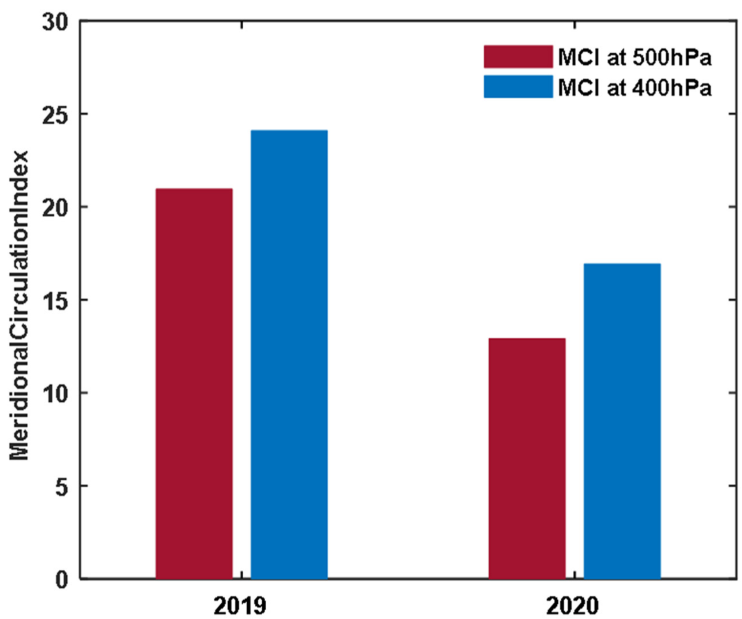

Figure 7. The meridional circulation index at 500 and 400 hPa in FMC_2019 and FMC_2020.

According to existing research, PBLH, temperature inversion, RH, and WS are the meteorological factors closely related to $PM_{2.5}$ [28,93], among which the difference of temperature between 900 and 1000 hPa ($T_{900}-T_{1000}$) refers to the temperature inversion and atmospheric stability [55,93]. Figure 8 and Table 5 show the fractional changes of the PBLH, $T_{900}-T_{1000}$, RH at 1000 hPa (RH_{1000}), and WS at 1000 hPa (WS_{1000}) between FMC_2020 and FMC_2019. It can be seen that in the BTH in FMC_2020, the PBLH has decreased by 24% and the lower PBLH allows $PM_{2.5}$ to mix in a smaller range; the $T_{900}-T_{1000}$ has increased by 13% and the stronger atmospheric stability is not conducive to the vertical diffusion of $PM_{2.5}$; the RH increases by 53% and the hygroscopic growth of $PM_{2.5}$ is strengthened; the WS decrease by 4% and horizontal diffusion of $PM_{2.5}$ is weakened. All of these meteorological factors are beneficial to the accumulation of air pollutants in the BTH. However, the four meteorological factors have different impacts on $PM_{2.5}$ changes in the CC, the YRD, and the PRD. The ±10% difference is used to take as a threshold of significance [55], which means that when the absolute values of fractional changes in meteorological factors are more than 10%, the meteorological factors may have a significant impact on $PM_{2.5}$ mass concentration. In the CC, the absolute values of fractional changes of PBLH, RH, and WS are less than 10%, and only $T_{900}-T_{1000}$ decreases by 22%. In the YRD, the absolute values of fractional changes of PBLH and RH are less than 10%, and $T_{900}-T_{1000}$ and WS decrease 17 and 26%, respectively. In general, the comprehensive effects of these changed meteorological elements on $PM_{2.5}$ changes are small in the CC and the YRD. In the PRD, PBLH increases by 8%, $T_{900}-T_{1000}$ decreases by 20%, WS increases by 18%, and RH increases a little (3%), all of which are beneficial to the diffusion of $PM_{2.5}$.

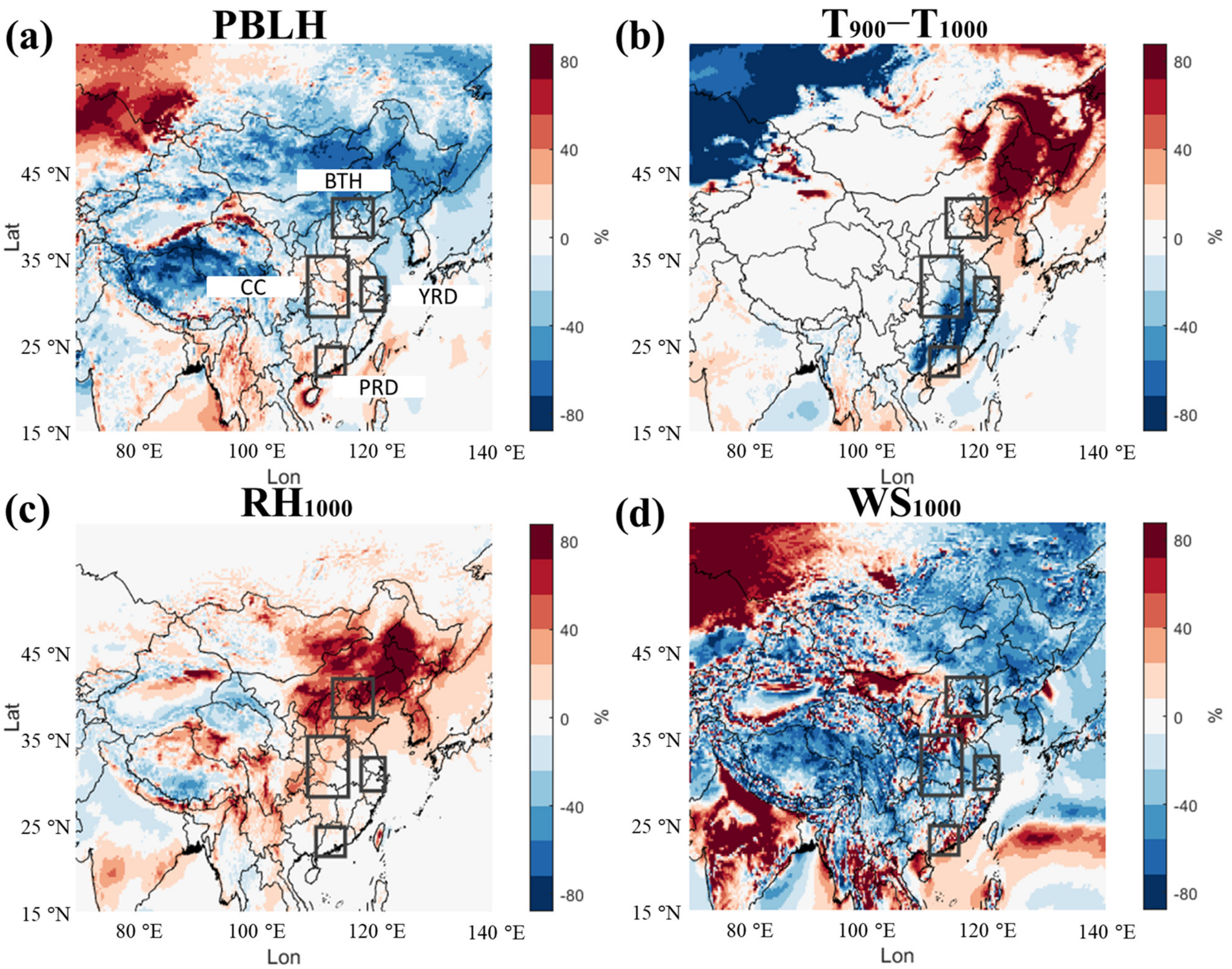

Figure 8. The fractional changes of the meteorological factors between FMC_2020 and FMC_2019 in China. (**a**) PBLH. (**b**) $T_{900}-T_{1000}$. (**c**) RH_{1000}. (**d**) WS_{1000}.

Table 5. The fractional changes of PBLH, $T_{900}-T_{1000}$, RH_{1000}, and WS_{1000}.

Area	PBLH	$T_{900}-T_{1000}$	RH_{1000}	WS_{1000}
BTH	−24%	13%	53%	−4%
CC	4%	−22%	8%	−7%
YRD	−8%	−17%	2%	−26%
PRD	8%	−20%	3%	18%

The contributions of changed meteorological conditions to $PM_{2.5}$ mass concentration can be derived from the difference between the two sensitive experiments. From Figure 9a–c, compared with FMC_2019, the overall meteorological conditions of FMC_2020 cause $PM_{2.5}$ mass concentration to increase by 35% (from 31 to 42 μg m^{-3}) in the BTH, 5% (from 28 to 29.5 μg m^{-3}) in the CC, and 6% (from 34 to 36 μg m^{-3}) in the YRD, which indicates that the meteorological conditions in FMC_2020 are more conducive to the accumulation of aerosol pollution. Besides, $PM_{2.5}$ mass concentration decreases by 8% (from 12 to 11 μg m^{-3}) in the PRD. This indicates that the meteorological conditions are more conducive to the diffusion of aerosol pollution.

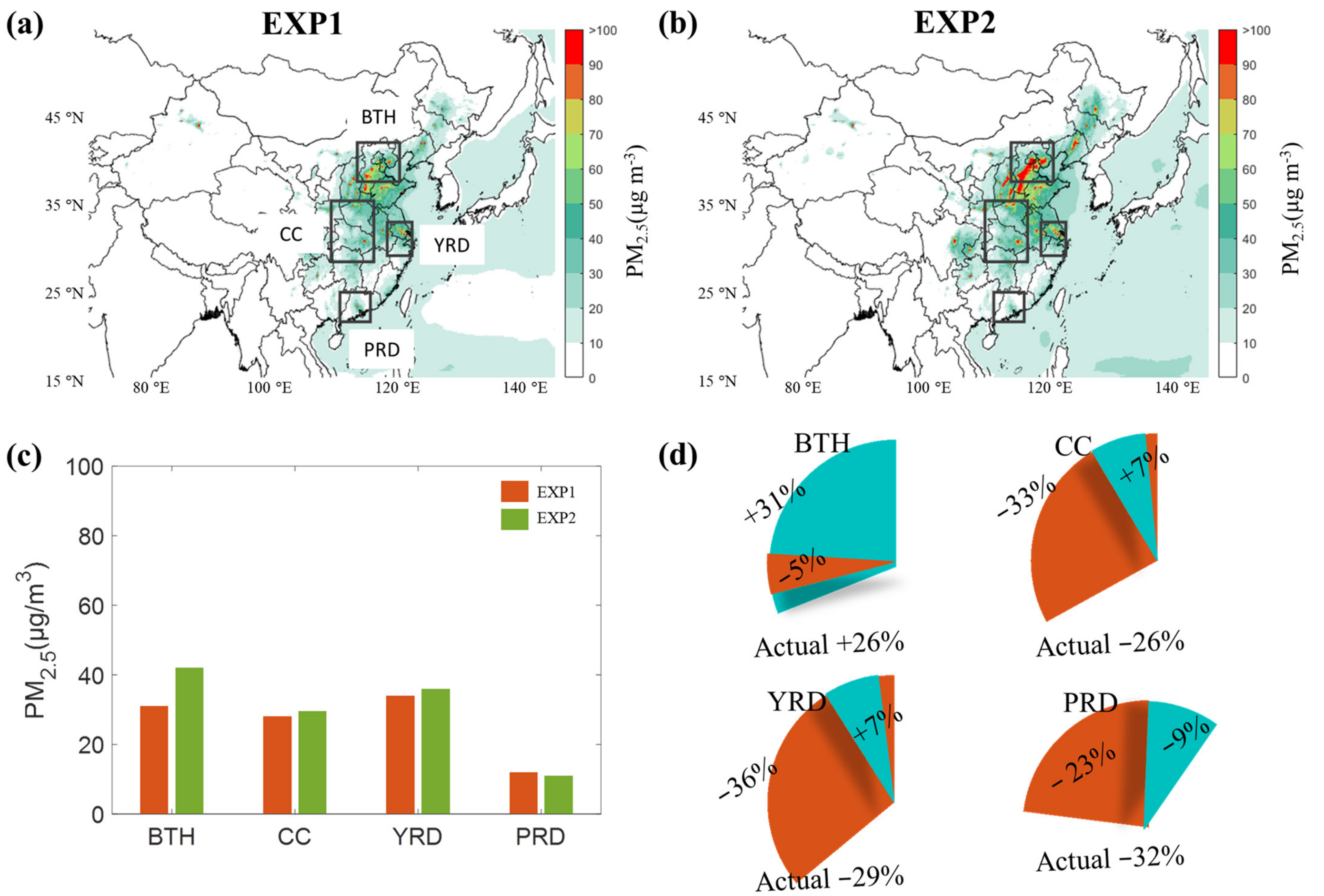

Figure 9. Simulated monthly average $PM_{2.5}$ mass concentration (μg m^{-3}) in China. (**a**) EXP1; (**b**) EXP2; (**c**) comparisons of $PM_{2.5}$ mass concentration between EXP1 and EXP2; (**d**) the relative contributions of changed emission and meteorological conditions to $PM_{2.5}$ mass concentration. The green parts and red parts in (**d**) represent meteorological conditions and emissions.

3.4. Relative Contributions of Emissions and Meteorological Conditions to $PM_{2.5}$ Changes

Assuming that the relationship between meteorology, emissions and $PM_{2.5}$ is linear is a widely used method to calculate the relative contributions of meteorology and emissions to $PM_{2.5}$ changes [94,95]. In Sections 3.2 and 3.3, the changes of $PM_{2.5}$ mass concentration caused by changed emissions and meteorological conditions are estimated, so the Equations (2) and (3) can be used to calculate the relative contributions of them to actual $PM_{2.5}$ mass concentration changes.

$$\mathrm{ReCON(met)} = \mathrm{AC(PM_{2.5})} \times \frac{\mathrm{CON(met)}}{\mathrm{CON(met)} + \mathrm{CON(emi)}} \tag{2}$$

$$\mathrm{ReCON(emi)} = \mathrm{AC(PM_{2.5})} \times \frac{\mathrm{CON(emis)}}{\mathrm{CON(met)} + \mathrm{CON(emi)}} \tag{3}$$

where $\mathrm{ReCON(met)}$ and $\mathrm{ReCON(emi)}$ represent the relative contributions of meteorological conditions and emissions to $PM_{2.5}$ mass concentration. $\mathrm{AC(PM_{2.5})}$ represents the actual changes of $PM_{2.5}$ mass concentration. $\mathrm{CON(met)}$ and $\mathrm{CON(emi)}$ represent the contributions of changed meteorological conditions and emissions to $PM_{2.5}$ mass concentration changes. The calculated results are shown in Figure 9d. The changed meteorological conditions and emissions cause $PM_{2.5}$ mass concentration to increase by 31% and decrease by 5% in the BTH, respectively, which indicates that meteorological conditions dominate the increase in $PM_{2.5}$ mass concentration. In the CC and the YRD, the changed emission causes the $PM_{2.5}$ mass concentration to decrease by 33 and 36%, respectively, which is much greater than the 7 and 7% increase from meteorology, reflecting the primary effect of the emissions. In the PRD, emissions and meteorology have caused $PM_{2.5}$ mass concentration to decrease by 23 and 9%.

4. Conclusions

The relative contributions of meteorological conditions and emissions to $PM_{2.5}$ changes are hot issues of air quality research in China. This paper uses air pollutants data, meteorological data, and the GRAPES_CUACE model to analyze and compare the relative contributions of emissions and meteorology on $PM_{2.5}$ changes in four different regions (the BTH, the CC, the YRD, and the PRD).

The results show that compared with FMC_2019, the $PM_{2.5}$ mass concentration in FMC_2020 in four regions has changed significantly. Among them, $PM_{2.5}$ mass concentration increases by 26% in the BTH while it decreases by 26, 29, and 32% in the CC, the YRD, and the PRD, respectively. These changes are mainly caused by the combined effects of changed emissions and meteorological conditions.

In terms of emissions, compared with FMC_2019, CO emissions have the smallest decrease in the BTH (4%), followed by the PRD (10%), the YRD (15%), and the CC (18%) in FMC_2020 by calculating the difference of CO mass concentration during periods associated with similar stable weather conditions. Besides, through using the linear regression equations with different r^2, the contributions of combustion sources to primary $PM_{2.5}$ in FMC_2020 increase by about 15% in the BTH and 18% in the CC, while decrease by 38% in the YRD and 83% in the PRD. The increased contributions in the BTH and the CC are caused by higher contributions of coal burning and emissions related to NO2, respectively. The decreased contributions of combustion sources in the YRD and the PRD are mainly related to the lower contributions of emissions related to SO_2.

For meteorology, compared with FMC_2019, the Siberian–Mongolian high-pressure is weakened, the high-pressure ridge at 500 hPa is strengthened, and the geopotential height lines are less dense in FMC_2020, which is not conducive to the diffusion of $PM_{2.5}$ in the BTH, the CC, and the YRD. However, the gradient of sea level pressure becomes larger in the PRD region, which is conducive to the diffusion of air pollutants. The MCI changes show that the air ventilation between the north and the south of China is weakened, which is not conducive to the diffusion of aerosol pollution in four regions. Moreover, PBLH decreases by 24%, the $T_{900}-T_{1000}$ increases by 13%, the RH increases by 53%, and the WS decreases by 4% in the BTH, which are all beneficial to the accumulation of aerosol pollution. However, meteorological factors have no significant changes in the CC and the YRD. In the PRD, meteorological factors are beneficial to the diffusion of aerosol pollution.

In general, in the BTH, the observed $PM_{2.5}$ mass concentration increase is mainly attributed to unfavorable meteorological conditions (+31%) which eliminate the −5% changes of $PM_{2.5}$ mass concentration caused by emissions reductions. In the CC and the YRD, the decrease in $PM_{2.5}$ mass concentration is dominated by emissions reductions (−33 and −36%), which are greater than the positive contributions of meteorological conditions (+7 and +7%). In the PRD, the decrease in $PM_{2.5}$ mass concentration is caused by emissions reductions (−23%) and favorable meteorological conditions (−9%). The changes in air pollutants in further pre-COVID years (Figures S1 and S2 from the Supplementary Materials) will continue to be discussed in future studies.

Supplementary Materials: The following supporting information can be downloaded at: https://www.mdpi.com/article/10.3390/atmos13020222/s1, Figure S1: Distributions of monthly average $PM_{2.5}$ mass concentration (μg m^{-3}) in China; Figure S2: Distributions of monthly average CO mass concentration (mg m^{-3}) in China; Figure S3: The values of CO/NO_x during FMC_2019 and FMC_2020 in the BTH; Figure S4: As in Figure S3, but in the CC; Figure S5: As in Figure S3, but in the YRD; Figure S6: As in Figure S3, but in the PRD.

Author Contributions: Conceptualization, H.W.; methodology, W.Z.; validation, W.Z., Y.P. and Z.L.; investigation, W.Z.; resources, Y.W. and H.C.; data curation, J.Z.; writing—review and editing, W.Z.; visualization, W.Z. and Y.Z.; supervision, H.W. and X.Z. All authors have read and agreed to the published version of the manuscript.

Funding: This study is supported by the National Key Research and Development Program of China (2019YFC0214601), the Major Program of National Natural Science Foundation of China (Grant No. 42090030).

Institutional Review Board Statement: Not applicable.

Informed Consent Statement: Not applicable.

Data Availability Statement: Not applicable.

Conflicts of Interest: The authors declare no conflict of interest. The funders had no role in the design of the study; in the collection, analyses, or interpretation of data; in the writing of the manuscript, or in the decision to publish the results.

References

1. Fu, G.Q.; Xu, W.Y.; Yang, R.F.; Li, J.B.; Zhao, C.S. The distribution and trends of fog and haze in the North China Plain over the past 30 years. *Atmos. Chem. Phys.* **2014**, *14*, 11949–11958. [CrossRef]
2. Li, Z.; Ma, Z.; van der Kuijp, T.J.; Yuan, Z.; Huang, L. A Review of Soil Heavy Metal Pollution from Mines in China: Pollution and Health Risk Assessment. *Sci. Total Environ.* **2013**, *468–469*, 843–853. [CrossRef] [PubMed]
3. Matus, K.; Nam, K.M.; Selin, N.E.; Lamsal, L.N.; Reilly, J.M.; Paltsev, S. Health damages from air pollution in China. *Glob. Environ. Chang.* **2012**, *22*, 55–66. [CrossRef]
4. Che, H.; Zhang, X.-Y.; Xia, X.; Goloub, P.; Holben, B.; Zhao, H.; Wang, Y.; Wang, H.; Blarel, L.; Damiri, B.; et al. Ground-based aerosol climatology of China: Aerosol optical depths from the China Aerosol Remote Sensing Network (CARSNET) 2002–2013. *Atmos. Chem. Phys.* **2015**, *15*, 7619–7652. [CrossRef]
5. Chen, H.; Wang, H. Haze Days in North China and the associated atmospheric circulations based on daily visibility data from 1960 to 2012. *J. Geophys. Res. Atmos.* **2015**, *120*, 5895–5909. [CrossRef]
6. Querol, X.; Alastuey, A.; Rodriguez, S.; Plana, F.; Ruiz, C.R. Monitoring of PM_{10} and $PM_{2.5}$ around primary particulate anthropogenic emission sources. *Atmos. Environ.* **2001**, *35*, 845–858. [CrossRef]
7. Zhang, Q.; Streets, D.G.; He, K.; Klimont, Z. Major components of China's anthropogenic primary particulate emissions. *Environ. Res. Lett.* **2007**, *2*, 045027. [CrossRef]
8. Zhai, S.; Jacob, D.; Wang, X.; Shen, L.; Ke, L.; Zhang, Y.; Gui, K.; Zhao, T.; Liao, H. Fine particulate matter ($PM_{2.5}$) trends in China, 2013–2018: Separating contributions from anthropogenic emissions and meteorology. *Atmos. Chem. Phys.* **2019**, *19*, 11031–11041. [CrossRef]
9. Jin, Q.; Fang, X.; Wen, B.; Shan, A. Spatio-temporal variations of $PM_{2.5}$ emission in China from 2005 to 2014. *Chemosphere* **2017**, *183*, 429–436. [CrossRef]

10. Andersson, A.; Deng, J.; Du, K.; Yan, C.; Zheng, M.; Sköld, M.; Gustafsson, O. Regionally-Varying Combustion Sources of the January 2013 Severe Haze Events over Eastern China. *Environ. Sci. Technol.* **2015**, *49*, 2038–2043. [CrossRef]
11. Pui, D.Y.H.; Chen, S.-C.; Zuo, Z. $PM_{2.5}$ in China: Measurements, sources, visibility and health effects, and mitigation. *Particuology* **2014**, *13*, 1–26. [CrossRef]
12. Cheng, S.; Lang, J.; Zhou, Y.; Han, L.; Wang, G.; Chen, D. A new monitoring-simulation-source apportionment approach for investigating the vehicular emission contribution to the $PM_{2.5}$ pollution in Beijing, China. *Atmos. Environ.* **2013**, *79*, 308–316. [CrossRef]
13. Zhang, T.; Claeys, M.; Cachier, H.; Dong, S.; Wang, W.; Maenhaut, W.; Liu, X. Identification and estimation of the biomass burning contribution to Beijing aerosol using levoglucosan as a molecular marker. *Atmos. Environ.* **2008**, *42*, 7013–7021. [CrossRef]
14. Liu, P.; Zhang, C.; Xue, C.; Mu, Y.; Liu, J.; Zhang, Y.; Tian, D.; Ye, C.; Zhang, H.; Guan, J. The contribution of residential coal combustion to atmospheric $PM_{2.5}$ in northern China during winter. *Atmos. Chem. Phys.* **2017**, *17*, 11503–11520. [CrossRef]
15. Zhang, Z.; Wang, W.; Cheng, M.; Liu, S.; Xu, J.; He, Y.; Meng, F. The contribution of residential coal combustion to $PM_{2.5}$ pollution over China's Beijing-Tianjin-Hebei region in winter. *Atmos. Environ.* **2017**, *159*, 147–161. [CrossRef]
16. Xu, Q.; Wang, S.; Jiang, J.; Bhattarai, N.; Li, X.; Chang, X.; Qiu, X.; Zheng, M.; Hua, Y.; Hao, J. Nitrate dominates the chemical composition of $PM_{2.5}$ during haze event in Beijing, China. *Sci. Total Environ.* **2019**, *689*, 1293–1303. [CrossRef] [PubMed]
17. Zhang, Q.; Quan, J.; Tie, X.; Li, X.; Liu, Q.; Gao, Y.; Zhao, D. Effects of meteorology and secondary particle formation on visibility during heavy haze events in Beijing, China. *Sci. Total Environ.* **2015**, *502*, 578–584. [CrossRef] [PubMed]
18. Cheng, Y.; Zheng, G.; Wei, C.; Mu, Q.; Zheng, B.; Wang, Z.; Gao, M.; Zhang, Q.; He, K.; Carmichael, G.; et al. Reactive nitrogen chemistry in aerosol water as a source of sulfate during haze events in China. *Sci. Adv.* **2016**, *2*, e1601530. [CrossRef] [PubMed]
19. Sun, Y.; Lei, L.; Zhou, W.; Chen, C.; He, Y.; Sun, J.; Li, Z.; Xu, W.; Wang, Q.; Ji, D.; et al. A chemical cocktail during the COVID-19 outbreak in Beijing, China: Insights from six-year aerosol particle composition measurements during the Chinese New Year holiday. *Sci. Total Environ.* **2020**, *742*, 140739. [CrossRef]
20. Huang, R.-J.; Zhang, Y.; Bozzetti, C.; Ho, K.-F.; Cao, J.-J.; Han, Y.; Daellenbach, K.R.; Slowik, J.G.; Platt, S.M.; Canonaco, F.; et al. High secondary aerosol contribution to particulate pollution during haze events in China. *Nature* **2014**, *514*, 218–222. [CrossRef]
21. Zhang, X.; Xu, X.; Ding, Y.; Liu, Y.; Zhang, H.; Wang, Y.; Zhong, J. The impact of meteorological changes from 2013 to 2017 on $PM_{2.5}$ mass reduction in key regions in China. *Sci. China Earth Sci.* **2019**, *62*, 1885–1902. [CrossRef]
22. Leibensperger, E.; Mickley, L.; Jacob, D. Sensitivity of US air quality to mid-latitude cyclone frequency and implications of 1980–2006 climate change. *Atmos. Chem. Phys.* **2008**, *8*, 7075–7086. [CrossRef]
23. Li, Q.; Jacob, D.J.; Park, R.; Wang, Y.; Heald, C.L.; Hudman, R.; Yantosca, R.M.; Martin, R.V.; Evans, M. North American pollution outflow and the trapping of convectively lifted pollution by upper-level anticyclone. *J. Geophys. Res. Atmos.* **2005**, *110*, D10301. [CrossRef]
24. Wu, P.; Ding, Y.; Liu, Y. Atmospheric circulation and dynamic mechanism for persistent haze events in the Beijing–Tianjin–Hebei region. *Adv. Atmos. Sci.* **2017**, *34*, 429–440. [CrossRef]
25. Liao, T.; Wang, S.; Ai, J.; Gui, K.; Duan, B.; Zhao, Q.; Zhang, X.; Jiang, W.; Sun, Y. Heavy pollution episodes, transport pathways and potential sources of $PM_{2.5}$ during the winter of 2013 in Chengdu (China). *Sci. Total Environ.* **2017**, *584–585*, 1056–1065. [CrossRef] [PubMed]
26. Liu, J.; Man, R.; Ma, S.; Li, J.; Wu, Q.; Peng, J. Atmospheric levels and health risk of polycyclic aromatic hydrocarbons (PAHs) bound to $PM_{2.5}$ in Guangzhou, China. *Mar. Pollut. Bull.* **2015**, *100*, 134–143. [CrossRef]
27. Wang, M.; Cao, C.; Li, G.; Singh, R.P. Analysis of a severe prolonged regional haze episode in the Yangtze River Delta, China. *Atmos. Environ.* **2015**, *102*, 112–121. [CrossRef]
28. Wang, H.; Li, J.; Peng, Y.; Zhang, M.; Che, H.; Zhang, X. The impacts of the meteorology features on $PM_{2.5}$ levels during a severe haze episode in central-east China. *Atmos. Environ.* **2019**, *197*, 177–189. [CrossRef]
29. Zhang, Y.; Chen, J.; Yang, H.; Li, R.; Yu, Q. Seasonal variation and potential source regions of $PM_{2.5}$-bound PAHs in the megacity Beijing, China: Impact of regional transport. *Environ. Pollut.* **2017**, *231*, 329–338. [CrossRef]
30. Mu, Q.; Liao, H. Simulation of the interannual variations of aerosols in China: Role of variations in meteorological parameters. *Atmos. Chem. Phys.* **2014**, *14*, 9597–9612. [CrossRef]
31. Zhong, J.; Zhang, X.; Wang, Y.; Sun, J.; Zhang, Y.; Wang, J.; Tan, K.; Shen, X.; Che, H.; Zhang, L.; et al. Relative contributions of boundary-layer meteorological factors to the explosive growth of $PM_{2.5}$ during the red-alert heavy pollution episodes in Beijing in December 2016. *J. Meteorol. Res.* **2017**, *31*, 809–819. [CrossRef]
32. Zhong, J.; Zhang, X.; Dong, Y.; Wang, Y.; Liu, C.; Wang, J.; Zhang, Y.; Che, H. Feedback effects of boundary-layer meteorological factors on cumulative explosive growth of $PM_{2.5}$ during winter heavy pollution episodes in Beijing from 2013 to 2016. *Atmos. Chem. Phys.* **2018**, *18*, 247–258. [CrossRef]
33. Zhong, J.; Zhang, X.; Wang, Y.; Wang, J.; Shen, X.; Zhang, H.; Wang, T.; Xie, Z.; Liu, C.; Chang, H.; et al. The two-way feedback mechanism between unfavorable meteorological conditions and cumulative aerosol pollution in various haze regions of China. *Atmos. Chem. Phys.* **2019**, *19*, 3287–3306. [CrossRef]
34. Liu, L.; Zhang, X.; Zhong, J.; Wang, J.; Yang, Y. The 'two-way feedback mechanism' between unfavorable meteorological conditions and cumulative $PM_{2.5}$ mass existing in polluted areas south of Beijing. *Atmos. Environ.* **2019**, *208*, 1–9. [CrossRef]

35. Zhang, W.; Zhang, X.; Zhong, J.; Wang, Y.; Wang, J.; Zhao, Y.; Bu, S. The effects of the “two-way feedback mechanism” on the maintenance of persistent heavy aerosol pollution over areas with relatively light aerosol pollution in northwest China. *Sci. Total Environ.* **2019**, *688*, 642–652. [CrossRef] [PubMed]
36. Chen, Z.; Chen, D.; Zhao, C.; Kwan, M.-P.; Cai, J.; Zhuang, Y.; Zhao, B.; Wang, X.; Chen, B.; Yang, J.; et al. Influence of meteorological conditions on $PM_{2.5}$ concentrations across China: A review of methodology and mechanism. *Environ. Int.* **2020**, *139*, 105558. [CrossRef]
37. Cai, S.; Wang, Y.; Zhao, B.; Wang, S.; Chang, X.; Hao, J. The impact of the “Air Pollution Prevention and Control Action Plan” on $PM_{2.5}$ concentrations in Jing-Jin-Ji region during 2012–2020. *Sci. Total Environ.* **2017**, *580*, 197–209. [CrossRef]
38. Wang, G.; Cheng, S.; Wei, W.; Yang, X.; Wang, X.; Jia, J.; Lang, J.; Lv, Z. Characteristics and emission-reduction measures evaluation of $PM_{2.5}$ during the two major events: APEC and Parade. *Sci. Total Environ.* **2017**, *595*, 81–92. [CrossRef]
39. Zhang, Q.; Zheng, Y.; Tong, D.; Shao, M.; Wang, S.; Zhang, Y.; Xu, X.; Wang, J.; He, H.; Liu, W. Drivers of improved $PM_{2.5}$; air quality in China from 2013 to 2017. *Proc. Natl. Acad. Sci. USA* **2019**, *116*, 24463. [CrossRef]
40. The State Council of the People’s Republic of China, The Eleventh Five-Year Plan for National Economic and Social Development of the People’s Republic of China. 2006. Available online: https://www.gov.cn/gongbao/content/2006/content_268766.htm (accessed on 8 May 2021). (In Chinese)
41. The State Council of the People’s Republic of China. The Twelfth Five-Year Plan for Energy Saving and Emission Reduction. Available online: https://www.gov.cn/2011lh/content_1824603.htm (accessed on 8 May 2021). (In Chinese)
42. The State Council of the People’s Republic of China. Air Pollution Prevention and Control Action Plan. Available online: https://www.gov.cn/zwgk/2013-09/12/content_2486773.htm (accessed on 8 May 2021). (In Chinese)
43. The State Council of the People’s Republic of China. Three-year Action Plan for Blue Skies. Available online: https://www.gov.cn/zhengce/content/2018-07/03/content_5303158.htm (accessed on 9 May 2021). (In Chinese)
44. Ansari, T.U.; Wild, O.; Li, J.; Yang, T.; Xu, W.; Sun, Y.; Wang, Z. Effectiveness of short-term air quality emission controls: A high-resolution model study of Beijing during the Asia-Pacific Economic Cooperation (APEC) summit period. *Atmos. Chem. Phys.* **2019**, *19*, 8651–8668. [CrossRef]
45. Zhang, L.; Shao, J.; Lu, X.; Zhao, Y.; Hu, Y.; Henze, D.K.; Liao, H.; Gong, S.; Zhang, Q. Sources and Processes Affecting Fine Particulate Matter Pollution over North China: An Adjoint Analysis of the Beijing APEC Period. *Environ. Sci. Technol.* **2016**, *50*, 8731–8740. [CrossRef] [PubMed]
46. Liu, T.; Gong, S.; He, J.; Yu, M.; Wang, Q.; Li, H.; Liu, W.; Zhang, J.; Li, L.; Wang, X.; et al. Attributions of meteorological and emission factors to the 2015 winter severe haze pollution episodes in China’s Jing-Jin-Ji area. *Atmos. Chem. Phys.* **2017**, *17*, 2971–2980. [CrossRef]
47. Ma, Q.; Wu, Y.; Zhang, D.; Wang, X.; Xia, Y.; Liu, X.; Tian, P.; Han, Z.; Xia, X.; Wang, Y.; et al. Roles of regional transport and heterogeneous reactions in the $PM_{2.5}$ increase during winter haze episodes in Beijing. *Sci. Total Environ.* **2017**, *599*, 246–253. [CrossRef] [PubMed]
48. Zhong, J.; Zhang, X.; Wang, Y. Reflections on the threshold for PM 2.5 explosive growth in the cumulative stage of winter heavy aerosol pollution episodes (HPEs) in Beijing. *Tellus Ser. B Chem. Phys. Meteorol.* **2018**, *71*, 1445379.
49. Chang, Y.; Huang, R.-J.; Ge, X.; Huang, X.; Hu, J.; Duan, Y.; Zou, Z.; Liu, X.; Lehmann, M. Puzzling Haze Events in China During the Coronavirus (COVID-19) Shutdown. *Geophys. Res. Lett.* **2020**, *47*, e2020GL088533. [CrossRef]
50. Huang, X.; Ding, A.; Gao, J.; Zheng, B.; Zhou, D.; Qi, X.; Tang, R.; Wang, J.; Ren, C.; Nie, W.; et al. Enhanced secondary pollution offset reduction of primary emissions during COVID-19 lockdown in China. *Natl. Sci. Rev.* **2020**, *8*, nwaa137. [CrossRef] [PubMed]
51. Tian, J.; Wang, Q.; Zhang, Y.; Yan, M.; Liu, H.; Zhang, N.; Ran, W.; Cao, J. Impacts of primary emissions and secondary aerosol formation on air pollution in an urban area of China during the COVID-19 lockdown. *Environ. Int.* **2021**, *150*, 106426. [CrossRef]
52. Le, T.; Wang, Y.; Liu, L.; Yang, J.; Yung, Y.L.; Li, G.; Seinfeld, J.H. Unexpected air pollution with marked emission reductions during the COVID-19 outbreak in China. *Science* **2020**, *369*, 702–706. [CrossRef]
53. Chu, B.; Zhang, S.; Liu, J.; Ma, Q.; He, H. Significant concurrent decrease in $PM_{2.5}$ and NO_2 concentrations in China during COVID-19 epidemic. *J. Environ. Sci.* **2021**, *99*, 346–353. [CrossRef]
54. Wang, Y.; Yuan, Y.; Wang, Q.; Liu, C.; Zhi, Q.; Cao, J. Changes in air quality related to the control of coronavirus in China: Implications for traffic and industrial emissions. *Sci. Total Environ.* **2020**, *731*, 139133. [CrossRef]
55. Wang, X.; Zhang, R. How Does Air Pollution Change during COVID-19 Outbreak in China? *Bull. Am. Meteorol. Soc.* **2020**, *101*, E1645–E1652. [CrossRef]
56. Zhao, N.; Wang, G.; Li, G.; Lang, J.; Zhang, H. Air pollution episodes during the COVID-19 outbreak in the Beijing–Tianjin–Hebei region of China: An insight into the transport pathways and source distribution. *Environ. Pollut.* **2020**, *267*, 115617. [CrossRef] [PubMed]
57. Li, M.; Wang, T.; Xie, M.; Li, S.; Zhuang, B.; Fu, Q.; Zhao, M.; Wu, H.; Liu, J.; Saikawa, E.; et al. Drivers for the poor air quality conditions in North China Plain during the COVID-19 outbreak. *Atmos. Environ.* **2021**, *246*, 118103. [CrossRef] [PubMed]
58. He, J.; Gong, S.; Yu, Y.; Yu, L.; Wu, L.; Mao, H.; Song, C.; Zhao, S.; Liu, H.; Li, X.; et al. Air pollution characteristics and their relation to meteorological conditions during 2014–2015 in major Chinese cities. *Environ. Pollut.* **2017**, *223*, 484–496. [CrossRef]

59. Li, M.; Zhang, Q.; Streets, D.; He, K.; Cheng, Y.; Emmons, L.; Huo, H.; Kang, S.C.; Lu, Z.; Shao, M.; et al. Mapping Asian anthropogenic emissions of non-methane volatile organic compounds to multiple chemical mechanisms. *Atmos. Chem. Phys.* **2014**, *14*, 5617–5638. [CrossRef]
60. Li, M.; Liu, H.; Geng, G.; Hong, C.; Liu, F.; Song, Y.; Tong, D.; Zheng, B.; Cui, H.; Man, H.; et al. Anthropogenic emission inventories in China:a review. *Natl. Sci. Rev.* **2017**, *4*, 834–866. [CrossRef]
61. Li, M.; Zhang, Q.; Kurokawa, J.-I.; Woo, J.-H.; He, K.; Lu, Z.; Ohara, T.; Song, Y.; Streets, D.G.; Carmichael, G.R.; et al. MIX: A mosaic Asian anthropogenic emission inventory under the international collaboration framework of the MICS-Asia and HTAP. *Atmos. Chem. Phys.* **2017**, *17*, 935–963. [CrossRef]
62. Lai, H.K.; Kendall, M.; Ferrier, H.; Lindup, I.; Alm, S.; Hänninen, O.; Jantunen, M.; Mathys, P.; Colvile, R.; Ashmore, M.; et al. Personal exposures and microenvironment concentrations of $PM_{2.5}$, VOC, NO_2 and CO in Oxford, UK. *Atmos. Environ.* **2004**, *38*, 6399–6410. [CrossRef]
63. Northcross, A.; Chowdhury, Z.; McCracken, J.; Canuz, E.; Smith, K. Estimating personal $PM_{2.5}$ exposures using CO measurements in Guatemalan households cooking with wood fuel. *J. Environ. Monit.* **2010**, *12*, 873–878. [CrossRef]
64. Bari, A.; Dutkiewicz, V.; Judd, C.; Wilson, L.; Luttinger, D.; Husain, L. Regional sources of particulate sulfate, SO_2, $PM_{2.5}$, HCl, and HNO_3, in New York, NY. *Atmos. Environ.* **2003**, *37*, 2837–2844. [CrossRef]
65. Song, H.; Zhang, Y.; Luo, M.; Gu, J.; Wu, M.; Xu, D.; Xu, G.; Ma, L. Seasonal variation, sources and health risk assessment of polycyclic aromatic hydrocarbons in different particle fractions of $PM_{2.5}$ in Beijing, China. *Atmos. Pollut. Res.* **2019**, *10*, 105–114. [CrossRef]
66. de Gouw, J.A.; Welsh-Bon, D.; Warneke, C.; Kuster, W.C.; Alexander, L.; Baker, A.K.; Beyersdorf, A.J.; Blake, D.R.; Canagaratna, M.; Celada, A.T.; et al. Emission and chemistry of organic carbon in the gas and aerosol phase at a sub-urban site near Mexico City in March 2006 during the MILAGRO study. *Atmos. Chem. Phys.* **2009**, *9*, 3425–3442. [CrossRef]
67. Wang, H.; Gong, S.; Zhang, H.; Chen, Y.; Shen, X.; Chen, D.; Xue, J.; Shen, Y.; Wu, X.; Jin, Z. A new-generation sand and dust storm forecasting system GRAPES_CUACE/Dust: Model development, verification and numerical simulation. *Chin. Sci. Bull.* **2010**, *55*, 635–649. [CrossRef]
68. Gong, S.; Zhang, X. CUACE/Dust–an integrated system of observation and modeling systems for operational dust forecasting in Asia. *Atmos. Chem. Phys.* **2008**, *8*, 2333–2340. [CrossRef]
69. An, X.Q.; Zhai, S.X.; Jin, M.; Gong, S.; Wang, Y. Development of an adjoint model of GRAPES–CUACE and its application in tracking influential haze source areas in north China. *Geosci. Model Dev.* **2016**, *9*, 2153–2165. [CrossRef]
70. Chen, D. Recent Progress on GRAPES Research and Application. *J. Appl. Meteorol. Sci.* **2006**, *17*, 773–777.
71. Chen, D.H.; Xue, J.; Yang, X.; Zhang, H.; Shen, X.; Hu, J.; Wang, Y.; Ji, L.; Chen, J. New generation of multi-scale NWP system (GRAPES): General scientific design. *Chin. Sci. Bull.* **2008**, *53*, 3433–3445. [CrossRef]
72. Zhang, R.H.; Shen, X. On the development of the GRAPES—A new generation of the national operational NWP system in China. *Chin. Sci. Bull.* **2008**, *53*, 3429–3432. [CrossRef]
73. Jiang, C.; Wang, H.; Zhao, T.; Li, T.; Che, H. Modeling study of $PM_{2.5}$ pollutant transport across cities in China's Jing–Jin–Ji region during a severe haze episode in December 2013. *Atmos. Chem. Phys.* **2015**, *15*, 5803–5814. [CrossRef]
74. Wang, H.; Shi, G.Y.; Zhang, X.Y.; Gong, S.L.; Tan, S.C.; Chen, B.; Che, H.Z.; Li, T. Mesoscale modelling study of the interactions between aerosols and PBL meteorology during a haze episode in China Jing–Jin–Ji and its near surrounding region–Part 2: Aerosols' radiative feedback effects. *Atmos. Chem. Phys.* **2015**, *15*, 3277–3287. [CrossRef]
75. Wang, H.; Xue, M.; Zhang, X.Y.; Liu, H.L.; Zhou, C.H.; Tan, S.C.; Che, H.Z.; Chen, B.; Li, T. Mesoscale modeling study of the interactions between aerosols and PBL meteorology during a haze episode in Jing–Jin–Ji (China) and its nearby surrounding region–Part 1: Aerosol distributions and meteorological features. *Atmos. Chem. Phys.* **2015**, *15*, 3257–3275. [CrossRef]
76. Zhang, W.; Wang, H.; Zhang, X.; Peng, Y.; Zhong, J.; Wang, Y.; Zhao, Y. Evaluating the contributions of changed meteorological conditions and emission to substantial reductions of $PM_{2.5}$ concentration from winter 2016 to 2017 in Central and Eastern China. *Sci. Total Environ.* **2020**, *716*, 136892. [CrossRef] [PubMed]
77. Chen, F.; Dudhia, J. Coupling an advanced land surface–hydrology model with the Penn State–NCAR MM5 modeling system. Part I: Model implementation and sensitivity. *Mon. Weather. Rev.* **2001**, *129*, 569–585. [CrossRef]
78. Hong, S.-Y.; Lim, J.-O.J. The WRF single-moment 6-class microphysics scheme (WSM6). *Asia-Pac. J. Atmos. Sci.* **2006**, *42*, 129–151.
79. Mlawer, E.J.; Taubman, S.J.; Brown, P.D.; Iacono, M.J.; Clough, S.A. Radiative transfer for inhomogeneous atmospheres: RRTM, a validated correlated-k model for the longwave. *J. Geophys. Res. Atmos.* **1997**, *102*, 16663–16682. [CrossRef]
80. Chou, M.-D.; Suarez, M.J.; Ho, C.-H.; Yan, M.M.H.; Lee, K.-T. Parameterizations for Cloud Overlapping and Shortwave Single-Scattering Properties for Use in General Circulation and Cloud Ensemble Models. *J. Clim.* **1998**, *11*, 202–214. [CrossRef]
81. Chen, F.; Janjić, Z.; Mitchell, K. Impact of Atmospheric Surface-layer Parameterizations in the new Land-surface Scheme of the NCEP Mesoscale Eta Model. *Bound. Layer Meteorol.* **1997**, *85*, 391–421. [CrossRef]
82. Hong, S.-Y.; Pan, H.-L. Nonlocal Boundary Layer Vertical Diffusion in a Medium-Range Forecast Model. *Mon. Weather. Rev.* **1996**, *124*, 2322–2339. [CrossRef]
83. Stockwell, W.R.; Middleton, P.; Chang, J.S.; Tang, X. The second generation regional acid deposition model chemical mechanism for regional air quality modeling. *J. Geophys. Res. Atmos.* **1990**, *95*, 16343–16367. [CrossRef]

84. Zhou, C.-H.; Gong, S.; Zhang, X.-Y.; Liu, H.-L.; Xue, M.; Cao, G.-L.; An, X.-Q.; Che, H.; Zhang, Y.-M.; Niu, T. Towards the improvements of simulating the chemical and optical properties of Chinese aerosols using an online coupled model–CUACE/Aero. *Tellus B Chem. Phys. Meteorol.* **2012**, *64*, 18965. [CrossRef]
85. Zhang, X.Y.; Wang, Y.Q.; Lin, W.L.; Zhang, Y.M.; Zhang, X.C.; Gong, S.; Zhao, P.; Yang, Y.Q.; Wang, J.Z.; Hou, Q.; et al. Changes of Atmospheric Composition and Optical Properties Over Beijing—2008 Olympic Monitoring Campaign. *Bull. Am. Meteorol. Soc.* **2009**, *90*, 1633–1652. [CrossRef]
86. Zhao, B.; Wang, S.; Wang, J.; Fu, J.S.; Liu, T.; Xu, J.; Fu, X.; Hao, J. Impact of national NOx and SO_2 control policies on particulate matter pollution in China. *Atmos. Environ.* **2013**, *77*, 453–463. [CrossRef]
87. Wang, G.; Zhang, R.; Gomez, M.E.; Yang, L.; Levy, Z.M.; Hu, M.; Lin, Y.; Peng, J.; Guo, S.; Meng, J.; et al. Persistent sulfate formation from London Fog to Chinese haze. *Proc. Natl. Acad. Sci. USA* **2016**, *48*, 13630–13635. [CrossRef]
88. Aneja, V.P.; Agarwal, A.; Roelle, P.A.; Phillips, S.B.; Tong, Q.; Watkins, N.; Yablonsky, R. Measurements and analysis of criteria pollutants in New Delhi, India. *Environ. Int.* **2001**, *27*, 35–42. [CrossRef]
89. Song, C.; Wu, L.; Xie, Y.; He, J.; Chen, X.; Wang, T.; Lin, Y.; Jin, T.; Wang, A.; Liu, Y.; et al. Air pollution in China: Status and spatiotemporal variations. *Environ. Pollut.* **2017**, *227*, 334–347. [CrossRef] [PubMed]
90. Shah, V.; Jaeglé, L.; Thornton, J.A.; Lopez-Hilfiker, F.D.; Lee, B.H.; Schroder, J.C.; Campuzano-Jost, P.; Jimenez, J.L.; Guo, H.; Sullivan, A.P.; et al. Chemical feedbacks weaken the wintertime response of particulate sulfate and nitrate to emissions reductions over the eastern United States. *Proc. Natl. Acad. Sci. USA* **2018**, *115*, 8110. [CrossRef] [PubMed]
91. Buchholz, S.; Junk, J.; Krein, A.; Heinemann, G.; Hoffmann, L. Air pollution characteristics associated with mesoscale atmospheric patterns in northwest continental Europe. *Atmos. Environ.* **2010**, *44*, 5183–5190. [CrossRef]
92. Liu, Z.; Wang, H.; Shen, X.; Peng, Y.; Shi, Y.; Che, H.; Wang, G. Contribution of Meteorological Conditions to the Variation in Winter $PM_{2.5}$ Concentrations from 2013 to 2019 in Middle-Eastern China. *Atmosphere* **2019**, *10*, 563. [CrossRef]
93. Zhong, J.; Zhang, X.; Wang, Y. Relatively weak meteorological feedback effect on $PM_{2.5}$ mass change in Winter 2017/18 in the Beijing area: Observational evidence and machine-learning estimations. *Sci. Total Environ.* **2019**, *664*, 140–147. [CrossRef]
94. Cheng, J.; Su, J.; Cui, T.; Li, X.; Dong, X.; Sun, F.; Yang, Y.; Tong, D.; Zheng, Y.; Li, Y.; et al. Dominant role of emission reduction in $PM_{2.5}$ air quality improvement in Beijing during 2013–2017: A model-based decomposition analysis. *Atmos. Chem. Phys.* **2019**, *19*, 6125–6146. [CrossRef]
95. Zhang, Q.; Jiang, X.; Tong, D.; Davis, S.J.; Zhao, H.; Geng, G.; Feng, T.; Zheng, B.; Lu, Z.; Streets, D.G.; et al. Transboundary health impacts of transported global air pollution and international trade. *Nature* **2017**, *543*, 705–709. [CrossRef] [PubMed]